

# Token-Shuffle: Towards High-Resolution Image Generation with Autoregressive Models

Xu Ma<sup>1\*</sup>, Peize Sun<sup>3</sup>, Haoyu Ma<sup>2</sup>, Hao Tang<sup>3</sup>, Chih-Yao Ma<sup>2</sup>, Jialiang Wang<sup>2</sup>, Kunpeng Li<sup>2</sup>, Xiaoliang Dai<sup>2</sup>, Yujun Shi<sup>4</sup>, Xuan Ju<sup>5</sup>, Yushi Hu<sup>6</sup>, Artsiom Sanakoyeu<sup>2</sup>, Felix Juefei-Xu<sup>2</sup>, Ji Hou<sup>2</sup>, Junjiao Tian<sup>2</sup>, Tao Xu<sup>2</sup>, Tingbo Hou<sup>2</sup>, Yen-Cheng Liu<sup>2</sup>, Zecheng He<sup>2</sup>, Zijian He<sup>2</sup>, Matt Feiszli<sup>3</sup>, Peizhao Zhang<sup>2</sup>, Peter Vajda<sup>2</sup>, Sam Tsai<sup>2</sup>, Yun Fu<sup>1</sup>

<sup>1</sup>Northeastern University, <sup>2</sup>Meta GenAI, <sup>3</sup>Meta FAIR, <sup>4</sup>National University of Singapore, <sup>5</sup>The Chinese University of Hong Kong, <sup>6</sup>University of Washington

\*Work done at Meta

Autoregressive (AR) models, long dominant in language generation, are increasingly applied to image synthesis but are often considered less competitive than diffusion-based models. A primary limitation is the substantial number of image tokens required for AR models, which constrains both training and inference efficiency, as well as image resolution. To address this, we present Token-Shuffle, a novel yet simple method that reduces the number of image tokens in Transformers. Our key insight is the dimensional redundancy of visual vocabularies in Multimodal Large Language Models (MLLMs), where low-dimensional visual codes from the visual encoder are directly mapped to high-dimensional language vocabularies. Leveraging this, we consider two key operations: *token-shuffle*, which merges spatially local tokens along channel dimension to decrease the input token number, and *token-unshuffle*, which untangles the inferred tokens after Transformer blocks to restore the spatial arrangement for output. Jointly training with textual prompts, our strategy requires no additional pretrained text-encoder and enables MLLMs to support extremely high-resolution image synthesis in a unified next-token prediction framework while maintaining efficient training and inference. For the first time, we push the boundary of AR text-to-image generation to a resolution of  $2048 \times 2048$  with impressive generation performance. In GenAI-benchmark, our 2.7B model achieves 0.77 overall score on hard prompts, outperforming AR models LlamaGen by 0.18 and diffusion models LDM by 0.15. Exhaustive large-scale human evaluations also demonstrate our superior image generation capabilities in terms of text-alignment, visual flaw, and visual appearance. We hope that Token-Shuffle can serve as a foundational design for efficient high-resolution image generation within MLLMs.

**Correspondence:** Xu Ma at [ma.xu1@northeastern.edu](mailto:ma.xu1@northeastern.edu)



## 1 Introduction

Within the framework of autoregressive Transformers, large language models (LLMs) Touvron et al. (2023b,a); Radford (2018) have recently achieved remarkable success in natural language processing by predicting the next token in a sequence. Building on these advances, recent efforts have aimed to expand LLMs with image generation capabilities Pan et al. (2025); Sun et al. (2024c); Wang et al. (2024b); Team (2024), leading to the development of multimodal large language models (MLLMs).

Two primary strategies are explored for image generation in MLLMs: *continuous* visual tokens Pan et al. (2025); Sun et al. (2024c); Li et al. (2024b) and *discrete* visual tokens Sun et al. (2024c); Wang et al. (2024b); Team (2024); Liu et al. (2024), each with unique pros and cons. Recent studies Fan et al. (2024) highlight that continuous tokens deliver superior image quality and require fewer tokens, offering notable computational efficiency. In contrast, discrete tokens generally produce lower visual quality and require a quadratic increase in token count with respect to image resolution. However, discrete tokens are more compatible with LLMs, as they only require an expanded vocabulary size to accommodate visual vocabularies. Continuous tokens, on the other hand, necessitate extensive modifications to the LLM pipeline, including additional loss functions (*e.g.*, regression Sun et al. (2024c) or diffusion loss Li et al. (2024b)), adjustments to causal masking Li et al.



**Figure 1** High-resolution images generated by our 2.7B AR model with Token-Shuffle (shuffle window size = 2).

(2024b); Fan et al. (2024), and significant engineering efforts (*e.g.*, model and loss parallelism). In addition, no strong evidence show that the continuous pipeline has less impact on text generation in MLLMs. Consequently, large-scale, real-world MLLM applications like EMU3 Wang et al. (2024b) and Chameleon Team (2024) predominantly adopt discrete visual tokens in practice.

Without altering the standard causal Transformers, discrete visual token MLLMs have explored applying the "next-token prediction" paradigm to image generation. Examples include LlamaGen Sun et al. (2024a), Chameleon Team (2024), and EMU3 Wang et al. (2024b), which utilize vector quantization image tokenizers Van Den Oord et al. (2017); Esser et al. (2021) to convert images into discrete tokens, allowing autoregressive Transformers to generate images in a process similar to language generation. Although these MLLMs demonstrate impressive image generation capabilities, they face substantial limitations in terms of achievable resolution and the associated number of visual tokens. Unlike language, which typically requires a few dozen to a few hundred tokens, images demand far more—often thousands of tokens (*e.g.*, 4K visual tokens to generate a  $1024 \times 1024$  resolution image). Due to the quadratic computational complexity of Transformers, this huge token number requirement makes both training and inference prohibitively costly. As a result, most MLLMs are limited to generating low- or medium-resolution images Tian et al. (2024); Sun et al. (2024a); Wang et al. (2024b); Liu et al. (2024), which restricts their ability to fully leverage the benefits of high-resolution images, such as enhanced detail preservation and fidelity. In contrast, high-resolution image generation has advanced significantly within the domain of diffusion models Ren et al. (2024); Chen et al. (2024); He et al. (2023); Haji-Ali et al. (2023). While tentative efforts have been made towards efficient LLMs that support long-context generation (which also benefits high-resolution image generation), these typically involve architectural modifications Ding et al. (2023); Gu and Dao (2023); Peng et al. (2023); Katharopoulos et al. (2020), overlook off-the-shelf LLMs, or are optimized for language generation without leveraging the unique properties of images Gloeckle et al. (2024). Consequently, developing effective methods to scale image generation resolution with discrete visual tokens in MLLMs remains a key area of research.

To deal with this issue, we first look into the details of integrating visual tokens into the LLM vocabulary. As outlined above, the common practice is to concatenate the visual tokenizer codebook with the original LLM vocabulary to form a new multimodal vocabulary. While straightforward, this approach overlooks the intrinsic differences in dimensionality. For instance, in typical VQGAN implementations, the codebook vector

dimension is relatively low, *e.g.*, 256 [Esser et al. \(2021\)](#). This low dimensionality is proven to be sufficient to distinguish vectors and has been shown to enhance both codebook usage and reconstruction quality [Sun et al. \(2024a\); Yu et al. \(2021, 2023a\)](#). However, directly appending the visual tokenizer codebook to the LLM vocabulary results in a dramatic increase in vector dimension, reaching 3072 or 4096, or even higher. This drastic increase inevitably introduces ineffective dimensional redundancy for the added visual vocabulary, as we empirically demonstrated in Fig. 3.

Inspired by this, we introduce Token-Shuffle, a pair of plug-and-play operations designed for MLLMs that significantly reduces the number of visual tokens for computation, enhancing both efficiency and high-resolution image synthesis. Our method draws inspiration from the widely-used pixel-shuffle [Shi et al. \(2016\)](#) technique in super-resolution, fusing visual tokens along the channel by leveraging the visual vocabulary dimensional redundancy. Rather than learning and generating each visual token individually, we process and generate a set of tokens within local windows sequentially, as illustrated in Fig. 2. This approach results in a *drastic reduction* in the number of visual tokens for computation (*e.g.*, saving  $\sim 75\%$  of tokens when shuffle window size is set to 2) while maintaining high-quality generation. Fundamentally distinct from aggressive compression ratios on which conventional visual encoders rely, Token-Shuffle takes a novel approach by preserving fine-grained information and dynamically fusing tokens through the exploitation of visual dimensional redundancy. This strategy leads to enhanced image fidelity and details in generation. Comprehensive analysis is provided in Sec. B.4.

For the first time, Token-Shuffle pushes the boundaries of autoregressive image generation to a resolution of  $2048 \times 2048$  and makes it possible to go beyond, while still enjoying efficient training and inference. In addition to facilitating high-resolution image generation, Token-Shuffle preserves impressive generation quality. Using the 2.7B Llama model, we achieve an overall score of 0.62 on the GenEval benchmark [Ghosh et al. \(2024\)](#) and a VQAScore of 0.77 on the GenAI-bench [Li et al. \(2024a\)](#), clearly outperforming related autoregressive models and even surpassing strong diffusion models, thereby setting a new state-of-the-art result. Besides, large-scale human evaluations also demonstrate the effectiveness of our proposed methods. The effectiveness and efficiency of Token-Shuffle demonstrate the substantial potential of our method, empowering MLLMs with the capability for high-resolution, high-fidelity image generation and paving the way for surpassing diffusion-based approaches.

## 2 Related Work

**Text-to-Image Generation** aims to synthesize images based on class or textual prompts. Recently, diffusion-based models [Ho et al. \(2020a\); Song et al. \(2020b\); Rombach et al. \(2022\); Peebles and Xie \(2023\); Dai et al. \(2023\)](#) have delivered impressive results. Denoising diffusion probabilistic models (DDPM) [Ho et al. \(2020b\)](#) laid the foundation of diffusion models, while denoising diffusion implicit models (DDIM) [Song et al. \(2020a\)](#) introduced a more efficient and deterministic sampling process. Based on these, Latent diffusion models (LDM) [Rombach et al. \(2022\)](#) innovatively shifted diffusion from pixel space to the latent space of powerful pretrained autoencoders, and introduced textual guidance. Other techniques, such as classifier-free guidance [Ho](#)

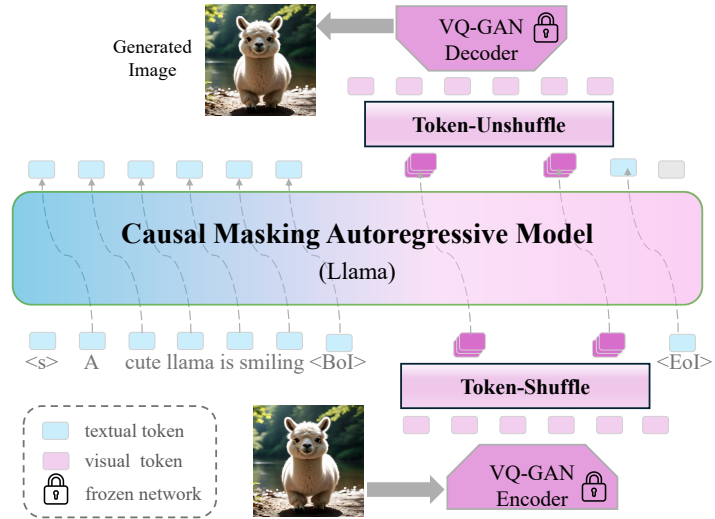


**Figure 2 Token-Shuffle Pipeline:** a plug-and-play operation pair for reducing visual token number in MLLMs, comprising a token-shuffle operation to merge spatially local visual tokens for Transformer input and a token-unshuffle operation to disentangle inferred visual tokens.

and Salimans (2022), Flow Matching Lipman et al. (2022); Polyak et al. (2024), and v-prediction Salimans and Ho (2022), have also contributed to improved image generation quality. Inspired by the success of Transformers in various tasks, recent approaches have explored Transformer designs for improved scalability, as demonstrated by models like DiT Peebles and Xie (2023) and U-ViT Bao et al. (2023). Moreover, work such as Imagen Saharia et al. (2022) has demonstrated the effectiveness of leveraging large language models (LLMs) for image synthesis. In our work, we take a different approach by directly exploring image synthesis using LLMs in an autoregressive manner, rather than diffusion-based methods.

**Autoregressive Models for Image Synthesis** have garnered significant attention recently. Unlike the dominant diffusion models, AR models offer the potential for a unified and general multimodal system. One of the recent works is LlamaGen Sun et al. (2024a), which employs a pure LLaMA Touvron et al. (2023a) architecture to generate images via *next-token prediction*. In contrast, the concurrent work VAR Tian et al. (2024) abandons next-token prediction in favor of next-scale prediction. Building on VAR, STAR Ma et al. (2024) integrates an additional text encoder and introduces textual guidance through cross-attention. Meanwhile, Open-MAGVIT2 Luo et al. (2024) highlights the benefits of a visual tokenizer with an extensive vocabulary. In a different approach, MAR Li et al. (2024b) eliminates the need for discrete visual tokens and instead uses a lightweight diffusion block to decode continuous latent features. However, the above approaches either focus on class-conditioned synthesis within predefined categories or rely on additional pretrained and frozen text encoders for text-conditioned synthesis. A unified autoregressive MLLM for text-conditioned image generation remains underexplored, and this is the focus of our work.

**Multimodal Large Language Models** are designed to understand and generate across various modalities Yu et al. (2023b). Given the recent wave of successes with LLMs Mann et al. (2020); Dubey et al. (2024), it is natural to extend LLMs into the multimodal domain. In such models, different modalities are encoded via specific tokenizers, fused, and jointly learned with other modalities. Conceptually, recent advances in multimodal models generally fall into two approaches: one uses continuous tokens for non-text modalities, and the other is based on discrete token representations for all modalities. For approaches with continuous tokens, they incorporate continuous features like VAE or CLIP Radford et al. (2021) features of visual data into LLMs for improved multimodal understanding and generation. These methods often result in better generation quality compared to discrete token-based models. As a result, numerous models have emerged, including EMU Sun et al. (2024c), EMU2 Sun et al. (2024b), SEED-X Ge et al. (2024), FLUID Fan et al. (2024), and MetaQueries Pan et al. (2025), etc. On the other hand, one of the leading models in the discrete token representation category is CM3Leon Yu et al. (2023b), which builds on the CM3 Aghajanyan et al. (2022) multimodal architecture. In addition to text and image generation and infilling, CM3Leon demonstrates the strong benefits of scaling and fine-tuning on diverse instruction-based datasets. Similar models, such as Chameleon Team (2024), EMU3 Wang et al. (2024b) and Lumina-mGPT Liu et al. (2024), have also shown promising results. In our work, we consider discrete tokens for MLLM image generation and target efficient high-resolution image generation.

## 3 Token-Shuffle

We present Token-Shuffle, a straightforward yet powerful method for reducing the number of visual tokens in MLLMs, significantly lowering computational costs and enabling efficient high-resolution image synthesis.

### 3.1 Preliminary

**Large Language Model Architecture** Our approach utilizes a decoder-only autoregressive Transformer model, specifically LLaMA Dubey et al. (2024), as the foundational language model. LLMs like LLaMA model the conditional probability of the  $t$ -th token  $\mathbb{P}(x_t|x_1, x_2, \dots, x_{t-1})$  through an autoregressive *next-token prediction* process, and only require the standard cross-entropy loss for training.

**Image Synthesis in LLMs** To enable LLMs to perform image synthesis, we incorporate discrete visual tokens into the model’s vocabulary. We utilize the pretrained VQGAN model from LlamaGen Sun et al. (2024a), which down-samples the input resolution by a factor of 16. The VQGAN codebook contains 16,384 tokens, which are concatenated with LLaMA’s original vocabulary. Additionally, special tokens <|start\_of\_image|> and

`<|end_of_image|>` are introduced to encapsulate the sequence of discrete visual tokens. During training, all tokens—including visual and textual—are used to compute the loss.

### 3.2 Limitations for Image synthesis

While various models have demonstrated the ability of image synthesis in MLLMs by inferring discrete visual tokens Sun et al. (2024a); Yu et al. (2023b); Wang et al. (2024b), an inevitable issue is the prohibitive number of visual tokens for high-resolution images. As aforementioned, to generate a high-resolution image with a resolution of  $1024 \times 1024$ , it requires a total of **4K** visual tokens if a down-sample 16 tokenizer is employed. Compared to language corpora, such a number of visual tokens makes the training extremely slow and the inference prohibitively inefficient. This will also largely restrict the generated image quality and aesthetic Sun et al. (2024a); Rombach et al. (2022). Moreover, if we increase the resolution to  $2048 \times 2048$ , it will correspondingly increase to **16K**, which is impractical for both effective training and efficient inference in the context of *next-token-prediction*.

In principle, increasing the number of visual tokens can yield more detailed, aesthetically pleasing images with higher resolution. However, this also introduces a prohibitive computational and inference burden. Previous approaches have always faced the trade-off: either enduring significantly increased training and inference costs, or sacrificing image resolution and quality. Addressing this dilemma is of particular interest in the field, as people seek methods that balance efficiency with high-fidelity image generation.

### 3.3 Visual Dimensional Redundancy

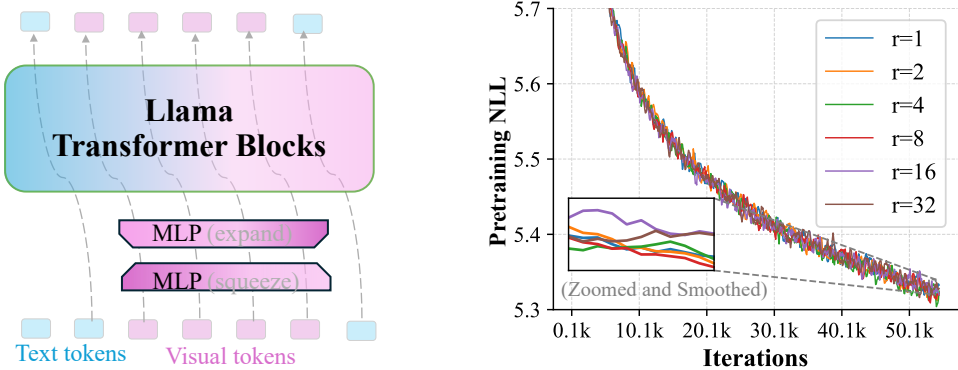


**Figure 3 Illustration of visual vocabulary dimensional redundancy.** **Left:** Two MLPs reduce visual token rank by a factor of  $r$ . **Right:** Pre-training loss (log-scaled perplexity) for different  $r$  values, showing substantial dimension reduction with minimal performance impact.

As illustrated above, a common strategy to endow large language models (LLMs) with image generation capabilities involves appending visual codebook tokens to the language vocabulary. While conceptually straightforward, this approach leads to a substantial increase in the embedding dimensionality for visual tokens. We contend that such a common approach of directly incorporating discrete visual tokens into the vocabulary of LLMs introduces inherent dimensional redundancy. To investigate this, we conduct a simple study using a 2.7B Llama-based MLLM with a dimension of 3072. For visual vocabularies, we introduce two linear layers to linearly reduce and expand the embedding dimension. This configuration ensures that the rank of the visual vocabulary is constrained to  $\frac{3072}{r}$ , where  $r$  is the compression factor. We train models with varying values of  $r$  on a licensed dataset for 55K iterations for demonstration. Fig. 3 shows that there is considerable redundancy in visual vocabularies, and we can compress the dimension by up to a factor of 8 without significantly impacting generation quality. A slight increase in loss is observed when larger compression factors are used.

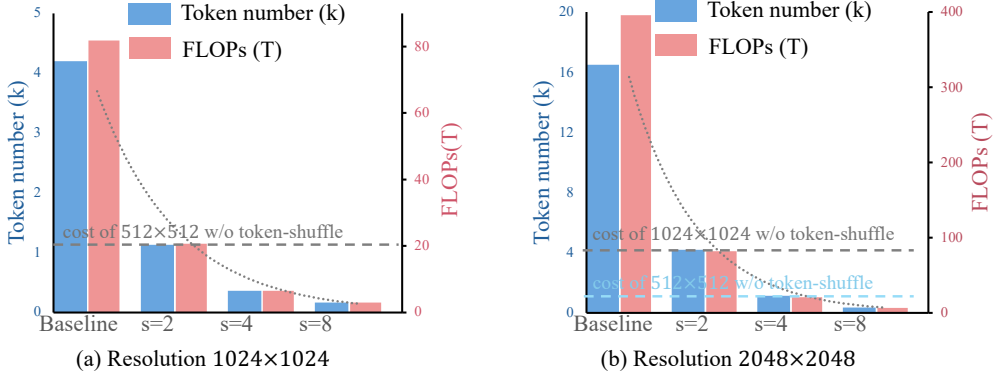


**Figure 4 Token-Shuffle can enhance efficiency quadratically.** For instance, with a shuffle window size  $s = 2$ , we achieve approximately a  $4\times$  reduction in both training FLOPs and token number. Considering the use of KV-cache during inference, inference time scales roughly linearly with the token number.

### 3.4 Token-Shuffle Operations

Motivated by our analysis of dimensional redundancy in visual vocabularies, we introduce **Token-Shuffle**—plug-and-play operations that reduce visual token counts in Transformer to improve computational efficiency and enable high-resolution image generation.

*Rather than reducing dimensional redundancy of visual vocabulary, we leverage this redundancy to reduce the number of visual tokens for greater efficiency.* Specifically, we shuffle spatially local visual tokens into a single token, then feed these fused visual tokens along with textual tokens into Transformer. A shared MLP layer is employed to compress visual token dimension, ensuring the fused token has same dimension as original. Assuming a local shuffle window size of  $s$ , our method reduces the token number by a factor of  $s^2$ , significantly alleviating the computational burden on the Transformer architecture. To recover the original visual tokens, we further introduce a token-unshuffle operation that disentangles the fused tokens back into their local visual tokens, with additional MLP layer to restore the original dimensionality. We also introduce residual MLP blocks in both operations. The entire Token-Shuffle pipeline is illustrated in Fig. 2 for clarity. *In essence, we do not reduce the number of tokens during inference or training but instead reduce the token count during Transformer computation.* Fig. 4 illustrates the efficiency of our proposed method. Moreover, rather than strictly adhering to the *next-token-prediction* paradigm, our approach predicts the *next fused token*, allowing us to output a set of local visual tokens in a single step, which significantly improves the efficiency and makes the high-resolution image generation feasible for AR models. See supplementary for analysis on causal attention.

### 3.5 Token-Shuffle Implementation Details

For Transformer input, we first compress the visual vocabulary dimension by a factor of  $s^2$  via an MLP layer that maps the dimension from  $d$  to  $\frac{d}{s^2}$ , where  $d$  represents the Transformer dimension. Next, local  $s \times s$  visual tokens are shuffled into a single token, reducing the total number of tokens per image from  $n$  to  $\frac{n}{s^2}$  while preserving the overall dimensionality. To enhance visual feature fusion, we add  $n$  MLP blocks. For Transformer output, we employ Token-Unshuffle. Here, MLP blocks map features into a new space, and an unshuffle operation expands each output visual token back to  $s \times s$  tokens. Another MLP layer then restores the dimension from  $\frac{d}{s^2}$  to  $d$ , with additional MLP blocks used to refine feature extraction. Consistently, both Token-Shuffle and Token-Unshuffle utilize  $n$  MLP layers for simplicity, where each MLP block consists of two linear projections with GELU activation. Further design choices for Token-Shuffle are explored in Sec 4.5.1.

### 3.6 CFG Scheduler for AR Image Generation

Following common practice Sun et al. (2024a); Wang et al. (2024b), we incorporate classifier-free guidance (CFG) Ho and Salimans (2022) during both training and inference, a technique widely used in the Diffusion community. During training, we randomly drop 10% of prompts, making the unconditional input format

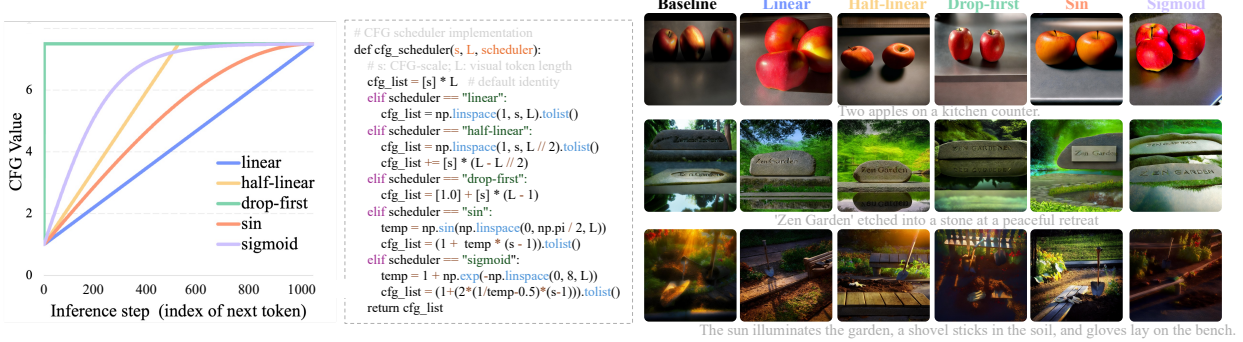


**Figure 5 Comparison of different CFG schedulers** with a monotonic increase in CFG scale from 1 to 7.5. **Right:** CFG-scheduler improves both visual aesthetics and text alignment, compared to the baseline of a consistent CFG value of 7.5 across all visual tokens.

<|begin\_of\_sentence|><|begin\_of\_image|> ... <|end\_of\_image|><|end\_of\_sentence|>. In inference, we adjust the logits of each visual token as  $l = l_{uncond} + \alpha(l_{cond} - l_{uncond})$  sequentially, where  $\alpha$  is a hyperparameter that controls the text-image alignment.

However, AR-based models differ fundamentally from diffusion-based models, and we argue that the vanilla CFG implementation may not be optimal for AR models. For unconditional input, generated image tokens are consistently conditioned on two system tokens, <|begin\_of\_sentence|> and <|begin\_of\_image|>. That is, the first unconditional logits always remain consistent, and applying the first fixed logits to conditional input logits may introduce unpredictable artifacts. These small errors accumulate auto-regressively from the first to the last token, potentially resulting in degraded image quality. Inspired by recent work Wang et al. (2024a), we further introduce a new inference CFG-scheduler to improve image generation quality. Our motivation is to minimize, or even eliminate, the influence of unconditional logits on early visual tokens to prevent artifacts. The cumulative impact of CFG from the first to last token would be enough to enhance both image quality and adherence to conditions. We explored several CFG-scheduler strategies, with results presented in Fig. 5 (zoom in for better visualization). Suggested by visual quality and human evaluation, we consider the half-linear scheduler for better generation by default.

## 4 Experiments

### 4.1 Training Details

We conduct all experiments using the 2.7B Llama model, which has a dimension of 3072 and consists of 20 autoregressive Transformer blocks. The models are trained on licensed dataset following Emu Dai et al. (2023). For training high-resolution images at  $2048 \times 2048$ , we exclude images with a resolution smaller than  $1024 \times 1024$ . Our model is initialized with the text pretrained 2.7B Llama checkpoint and begins training with a learning rate of  $2e^{-4}$ . All image captions are rewritten by Llama3 Dubey et al. (2024) to generate long prompts with details, which is demonstrated to be helpful for better generation.

We pre-train the models in three stages, from low-resolution to high-resolution image generation. First, we train the models using an image resolution of  $512 \times 512$  without employing the Token-Shuffle operation, as the number of visual tokens is not substantial at this stage. In this stage, we train on approximately 50 Billion tokens, using a sequence length of 4K, a global batch size of 512, and a total of 211K steps. Next, we scale the image resolution up to  $1024 \times 1024$  and introduce the Token-Shuffle operation to reduce the number of visual tokens for improved computational efficiency. In this stage, we scale up to 2 TB training tokens. Finally, we further scale up to  $2048 \times 2048$  using the previously trained checkpoint on around 300 Billion tokens with an initial learning rate of  $4e^{-5}$ . Unlike training on lower resolutions, *we observe that handling higher resolutions (e.g.,  $2048 \times 2048$ ) always results in unstable training, with the loss and gradient value increasing unexpectedly*. To address this, we incorporate z-loss Team (2024), which stabilizes training for very-high-resolution image generation. Detailed exploration and implementation specifics are provided in supplementary Sec. A. We fine-tune all models at different stages with a learning rate of  $4e^{-6}$  on 1,500 selected high-aesthetic quality

Model	Type	"Basic" prompts						"Hard" prompts					
		Attribute	Scene	Relation			Overall	Count	Differ	Compare	Logical		Overall
				Spatial	Action	Part					Negate	Universal	
SDXL-v2.1	Diff.	0.80	0.79	0.76	0.77	0.80	0.78	0.68	0.70	0.68	0.54	0.64	0.62
SD-XL Turbo	Diff.	0.85	0.85	0.80	0.82	0.89	0.84	0.72	0.74	0.70	0.52	0.65	0.65
DeepFloyd-IF <a href="#">Saharia et al. (2022)</a>	Diff.	0.83	0.85	0.81	0.82	0.89	0.84	0.74	0.74	0.71	0.53	0.68	0.66
Midjourney v6	Diff.	0.88	0.87	0.87	0.87	0.91	0.87	0.78	0.78	0.79	0.50	0.76	0.69
DALL-E 3 <a href="#">Betker et al. (2023)</a>	Diff.	0.91	0.90	0.92	0.89	0.91	<b>0.90</b>	0.82	0.78	0.82	0.48	0.80	0.70
LlamaGen <a href="#">Sun et al. (2024a)</a>	AR	0.75	0.75	0.74	0.76	0.75	0.74	0.63	0.68	0.69	0.48	0.63	0.59
Lumina-mGPT-7B <a href="#">Liu et al. (2024)</a>	AR	0.84	0.85	0.82	0.84	0.93	0.83	0.75	0.69	0.73	0.47	0.69	0.63
EMU3 <a href="#">Wang et al. (2024b)</a>	AR	0.78	0.81	0.77	0.78	0.87	0.78	0.69	0.62	0.70	0.45	0.69	0.60
SEED-X <a href="#">Ge et al. (2024)</a>	AR+Diff.	0.86	0.88	0.85	0.85	0.90	0.86	0.79	0.77	0.77	0.56	0.73	0.70
Token-Shuffle	AR	0.78	0.77	0.80	0.76	0.83	0.78	0.76	0.74	0.74	0.58	0.64	0.67
Token-Shuffle†	AR	0.88	0.88	0.88	0.87	0.91	0.88	0.81	0.82	0.81	0.68	0.78	<b>0.77</b>

**Table 1** VQAScore evaluation of image generation on GenAI-Bench. "†" indicates that images are generated by Llama3-rewritten prompts to match the caption length in the training data, for training-inference consistency.

Method	Type	# Params	Single Obj.	Two Obj.	Counting	Colors	Position	Color Attri.	Overall ↑
LDM <a href="#">Rombach et al. (2022)</a>	Diff.	1.4B	0.92	0.29	0.23	0.70	0.02	0.05	0.37
SDv1.5 <a href="#">Rombach et al. (2022)</a>	Diff.	0.9B	0.97	0.38	0.35	0.76	0.04	0.06	0.43
PixArt-alpha <a href="#">Chen et al. (2024)</a>	Diff.	0.6B	0.98	0.50	0.44	0.80	0.08	0.07	0.48
SDv2.1 <a href="#">Rombach et al. (2022)</a>	Diff.	0.9B	0.98	0.51	0.44	0.85	0.07	0.17	0.50
DALL-E 2 <a href="#">Ramesh et al. (2022)</a>	Diff.	6.5B	0.94	0.66	0.49	0.77	0.10	0.19	0.52
SDXL <a href="#">Podell et al. (2023)</a>	Diff.	2.6B	0.98	0.74	0.39	0.85	0.15	0.23	0.55
SD3 <a href="#">Esser et al. (2024)</a>	Diff.	2B	0.98	0.74	0.63	0.67	0.34	0.36	0.62
Show-o <a href="#">Xie et al. (2024b)</a>	AR.+Diff.	1.3B	0.95	0.52	0.49	0.82	0.11	0.28	0.53
SEED-X <a href="#">Ge et al. (2024)</a>	AR.+Diff.	17B	0.97	0.58	0.26	0.80	0.19	0.14	0.49
Transfusion <a href="#">Zhou et al. (2024)</a>	AR.+Diff.	7.3B	-	-	-	-	-	-	0.63
LlamaGen <a href="#">Sun et al. (2024a)</a>	AR.	0.8B	0.71	0.34	0.21	0.58	0.07	0.04	0.32
Chameleon Team <a href="#">(2024)</a>	AR.	7B	-	-	-	-	-	-	0.39
EMU3 <a href="#">Wang et al. (2024b)</a>	AR.	8B	-	-	-	-	-	-	0.66
EMU3-DPO <a href="#">Wang et al. (2024b)</a>	AR.	8B	-	-	-	-	-	-	0.64
Emu3-Gen <a href="#">Wang et al. (2024b)</a>	AR.	8B	0.98	0.71	0.34	0.81	0.17	0.21	0.54
Janus <a href="#">Wu et al. (2024)</a>	AR.	1.3B	0.97	0.68	0.30	0.84	0.46	0.42	0.61
Token-Shuffle†	AR.	2.7B	0.96	0.81	0.37	0.78	0.40	0.39	0.62

**Table 2** Evaluation on the GenEval benchmark. Similar to ours results, EMU3 and EMU3-DPO also consider prompt rewriting, and results of EMU3-Gen are from Janus [Wu et al. \(2024\)](#). These results indicate our Token-Shuffle can also present promising generation quality besides high-resolution.

images for presentation. By default, we present visualizations and evaluations based on the fine-tuned results at a resolution of  $1024 \times 1024$  and token-shuffle window size of 2, unless otherwise specified.

## 4.2 Quantitative Evaluation

While FID [Heusel et al. \(2017\)](#) or CLIPScore [Hessel et al. \(2021\)](#) are commonly used for image generation evaluation for class-conditioned synthesis, it is well-known that metrics are not reasonable for textual guided generation, as demonstrated in various related works [Lin et al. \(2024\)](#); [Ghosh et al. \(2024\)](#). In our work, we consider two benchmarks: GenEval [Ghosh et al. \(2024\)](#) and GenAI-Bench [Li et al. \(2024a\)](#). GenAI-Bench uses VQAScore [Lin et al. \(2024\)](#) as the auto-evaluation metric, which fine-tuned a visual-question-answering (VQA) model to produce an text-image alignment score. Since our training captions are long captions similar to LlamaGen [Sun et al. \(2024a\)](#), we report results based on Llama3-rewritten prompts for caption length consistency. Additionally, we include results from the original prompts for reference.

The results in Tab. 1 highlight the strong performance of our Token-Shuffle. Compared with other autoregressive models, our method outperforms LlamaGen by an overall score of 0.14 on "basic" prompts and 0.18 on "hard" prompts. Against strong diffusion-based baselines, our method surpasses DALL-E 3 by 0.7 in overall score on "hard" prompts.

Besides VQAScore results reported in Table 1, we also conduct additional auto-evaluation, GenEval, and report the detailed evaluation results in Table 2. All inference configurations are the same and we consider the rewritten prompt by default. Experimental results indicate that besides high-resolution, our Token-Shuffle, a pure AR-model, is able to present promising generation quality.

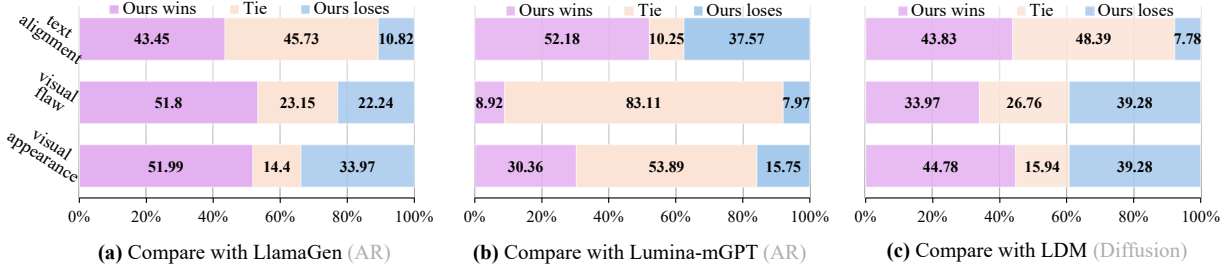


**Figure 6 Human evaluation** comparing Token-Shuffle with LlamaGen Sun et al. (2024a) (AR-based model without text), Lumina-mGPT Liu et al. (2024) (AR-based model with text) and LDM Rombach et al. (2022) (diffusion-based model) on text alignment, visual flaws, and visual appearance.

### 4.3 Human Evaluation

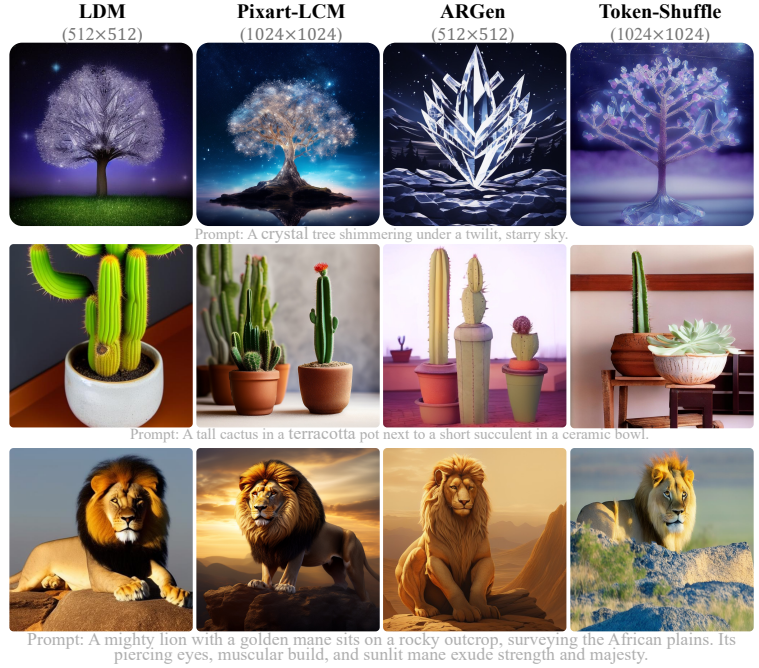
We recognize that while automated evaluation metrics provide unbiased assessments, they may not always fully capture human preferences, as suggested by recent studies Dai et al. (2023); Kirstain et al. (2023); Podell et al. (2023). To this end, we also conducted large-scale human evaluations on the GenAI-bench prompts set, comparing our model with LlamaGen Sun et al. (2024a), Lumina-mGPT Liu et al. (2024), and with LDM Rombach et al. (2022), as representative methods for AR model, MLLM, and Diffusion, respectively. For human evaluation, we focus on three key metrics: **text alignment**, assessing the accuracy with which images reflect textual prompts; **visual flaws**, checking for logical consistency to avoid issues such as incomplete bodies or extra limbs; and **visual appearance**, which evaluates the aesthetic quality of the images.

Fig. 6 presents the results, where our model consistently outperforms AR-based model LlamaGen and Lumina-mGPT across all evaluation aspects.

This suggests that Token-Shuffle effectively preserves aesthetic details and closely adheres to textual guidance with adequate training, even when token count is largely reduced for efficiency. In comparison with LDM, we demonstrate that AR-based MLLMs can achieve comparable or superior generation results (in terms of both visual appearance and text alignment) relative to Diffusion models. However, we observe that Token-Shuffle performs slightly worse than LDM in terms of visual flaws, consistent with observations in Fluid Fan et al. (2024), highlighting an interesting area for further exploration.

### 4.4 Visual Examples

We compare Token-Shuffle visually against other models, including two diffusion-based models, LDM and Pixart-LCM Chen et al. (2024), and one autoregressive model, LlamaGen Sun et al. (2024a). The visual examples are presented in Fig. 7. While all models exhibit favorable generation results, our Token-Shuffle appears to align more closely with the text, as demonstrated in rows 4 and 5. A possible reason for this is



**Figure 7 Visual comparison** with other open-source diffusion-based and AR-based models (zoom in for details).

that we jointly train text and image within a unified MLLM-style model. Compared to AR model LlamaGen, Token-Shuffle achieves higher resolution at the same inference cost, offering improved visual quality and text alignment. When compared to diffusion-based models, our AR-based model Token-Shuffle demonstrates competitive generation performance, while also supporting high-resolution outputs.

## 4.5 Ablation study

### 4.5.1 Design choice of Token-Shuffle

We acknowledge that similar implementations of Token-Shuffle or alternative methodologies may also be effective. Here, we explore and evaluate several variations:

- *More MLP blocks.* In the default setting, we use  $n = 2$  MLP blocks. To assess whether increasing the number of MLP blocks enhances performance, we experiment with configurations of  $n = 4$  and  $n = 6$ .
- *Shuffle or Drop.* To determine the importance of each token within local windows, we compare the standard Token-Shuffle operation with a variation in which all tokens in a local window are dropped except the last one.
- *Additional Positional Embedding.* As MLP layers are position-aware, we do not include additional positional embeddings in the default setup, and RoPE is already used in the Transformer blocks. To evaluate the potential benefits of additional positional embeddings, we introduce learnable embeddings at the local (shared and within shuffle-window) and global ranges, respectively.
- *Re-sampler and Simple version.* We further explore re-sampler Ge et al. (2024) to fuse and decouple tokens, replacing the Token-Shuffle design. In addition, we follow the common practice for high-resolution image understanding in Vision-Language Models, which directly concatenates local visual features and use MLP to match dimension. For outputs, we first use an MLP to expand the dimension and then decouple the tokens. We term this option as simple version. Notice that all operations in simple version are linear.

For a fair comparison, we standardize all training configurations across these experiments. All models are trained for 60K iterations on 32 GPUs with a learning rate of  $2 \times 10^{-4}$ , a sequence length of 4096, and a batch size of 4. We conduct experiments at a resolution of  $512 \times 512$ , using a Token-Shuffle window size of 2 for all model variants. This setup allows us to directly compare training loss to evaluate the effectiveness of each design choice.

As shown in Fig. 9, the training loss (log-scaled perplexity, which is commonly used evaluation for pretraining stage) suggests that our default configuration is a reasonable choice for implementing Token-Shuffle. In Fig. 9a, we observe that adding more MLP blocks in the Token-Shuffle operations (for both input and output) does not lead to noticeable improvements. Additionally, Fig. 9b illustrates that retaining all visual tokens is

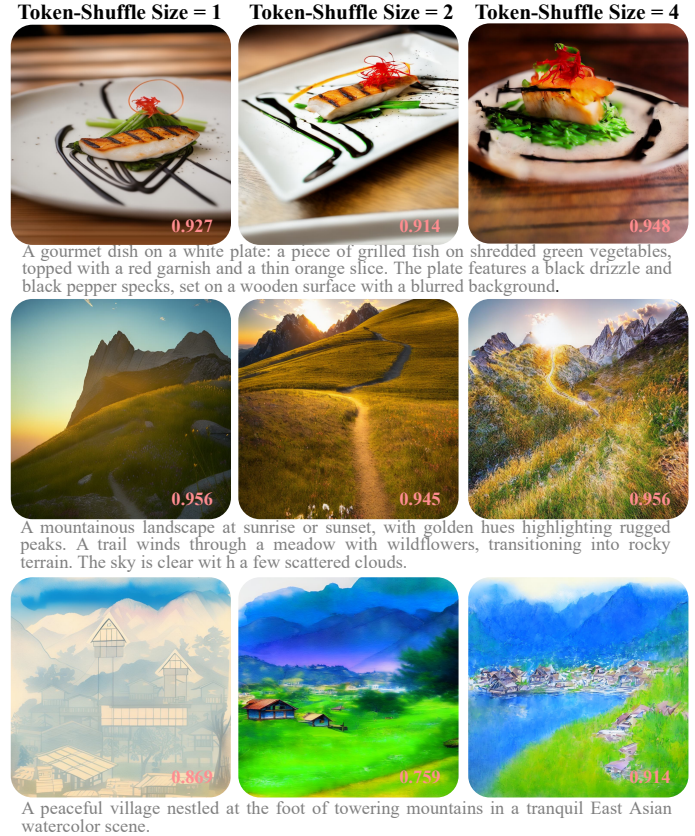


**Figure 8** Visual comparison of different Token-Shuffle window sizes. We tested each prompt with fixed random seeds and reported the VQAScore Lin et al. (2024) in the bottom-right corner.

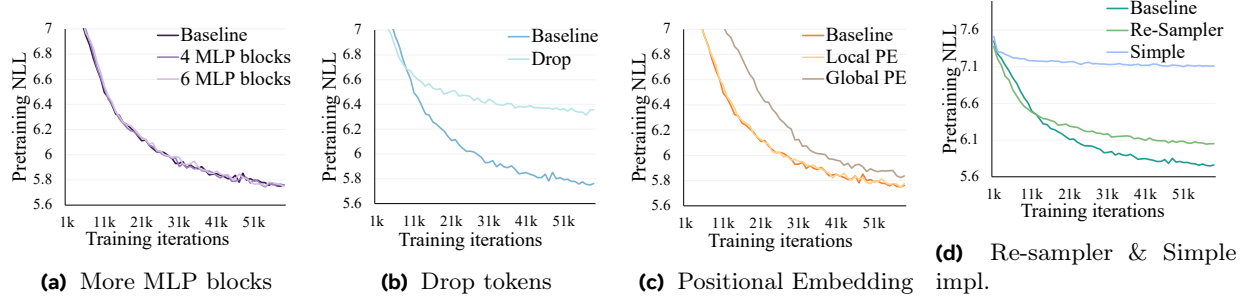


**Figure 9** Effectiveness comparison of various Token-Shuffle implementations and alternatives. Our implementation shows reasonable alignment with the Token-Shuffle concept, as indicated by the training loss in a fair comparison.

crucial. Our experiments further reveal that additional positional embeddings do not enhance Token-Shuffle, likely because MLP layers are inherently position-aware and RoPE is already employed to model relative positional information among fused visual tokens. We also observe that the Re-sampler performs worse than our Token-Shuffle as demonstrated in Fig. 9d; this may be due to our Re-sampler’s design, which is forced for local fusion and disentanglement, differing from original Re-sampler in SEED-X and related works. Meanwhile, the simplified version of our method performs the worst, even though it introduces more parameters, possibly due to the linear projection and overly simplified output design — an area for further investigation.

#### 4.5.2 Comparison of different shuffle sizes

Our Token-shuffle enjoys flexible settings of Token-Shuffle window size, like 1, 2, 4, and even larger, resulting in different levels of token compression and efficiency boosts. However, we acknowledge that larger Token-Shuffle window size will certainly decrease generation quality due to significantly reduced computations in Transformer. Here, we investigate the impact of different shuffle window sizes in Fig. 10.

Note that a shuffle window size of 1 implies that no Token-Shuffle is applied, though additional MLP layers are still introduced. As expected, increasing the shuffle window size leads to higher training loss and a corresponding reduction in generation quality. This is a logical and anticipated phenomenon, as a single fused token represents an increasingly larger number of visual tokens and significant computational reduction for Transformer. Exploring methods to minimize the gap in quality and training loss remains an important area of interest. Fig. 8 illustrates the differences in generated images across various shuffle sizes, with each image labeled with its VQAScore Lin et al. (2024). When the shuffle size is small, such as 1 or 2, the generated images exhibit excellent quality. With larger shuffle sizes, while high-fidelity images are still achievable, a slight blurring effect is noticed. Extended training could potentially help mitigate this issue.

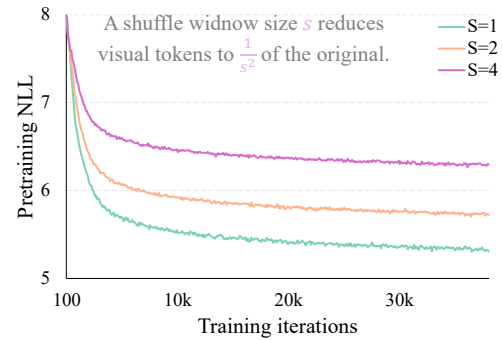


**Figure 10** Training losses for different shuffle window sizes.

This is a logical and anticipated phenomenon, as a single fused token represents an increasingly larger number of visual tokens and significant computational reduction for Transformer. Exploring methods to minimize the gap in quality and training loss remains an important area of interest. Fig. 8 illustrates the differences in generated images across various shuffle sizes, with each image labeled with its VQAScore Lin et al. (2024). When the shuffle size is small, such as 1 or 2, the generated images exhibit excellent quality. With larger shuffle sizes, while high-fidelity images are still achievable, a slight blurring effect is noticed. Extended training could potentially help mitigate this issue.

## 5 Conclusion

In this work, we introduce Token-Shuffle for efficient and scalable image generation in MLLMs. Unlike prior methods that rely on high compression ratios or reduced visual token inputs, we shuffle spatially local visual tokens for input and unshuffle the fused tokens back for output. Token-Shuffle is a lightweight, plug-and-play design for MLLMs that adheres to the next-token prediction paradigm while enabling batch generation of tokens within a local window. Our Token-Shuffle significantly reduces computational cost and accelerates inference. Leveraging these advantages, for the first time, we push the boundaries of autoregressive text-to-image generation to a resolution of  $2048 \times 2048$ , achieving high efficiency in training and inference at low cost while maintaining promising generation quality. As a tentative exploration, we anticipate further advancements toward scalable image generation for autoregressive models.

## References

- Armen Aghajanyan, Bernie Huang, Candace Ross, Vladimir Karpukhin, Hu Xu, Naman Goyal, Dmytro Okhonko, Mandar Joshi, Gargi Ghosh, Mike Lewis, et al. Cm3: A causal masked multimodal model of the internet. *arXiv preprint arXiv:2201.07520*, 2022.
- Fan Bao, Shen Nie, Kaiwen Xue, Yue Cao, Chongxuan Li, Hang Su, and Jun Zhu. All are worth words: A vit backbone for diffusion models. In *Proceedings of the IEEE/CVF conference on computer vision and pattern recognition*, pages 22669–22679, 2023.
- James Betker, Gabriel Goh, Li Jing, Tim Brooks, Jianfeng Wang, Linjie Li, Long Ouyang, Juntang Zhuang, Joyce Lee, Yufei Guo, et al. Improving image generation with better captions. *Computer Science*. <https://cdn.openai.com/papers/dall-e-3.pdf>, 2(3):8, 2023.
- Junsong Chen, Chongjian Ge, Enze Xie, Yue Wu, Lewei Yao, Xiaozhe Ren, Zhongdao Wang, Ping Luo, Huchuan Lu, and Zhenguo Li. Pixart- $\sigma$ : Weak-to-strong training of diffusion transformer for 4k text-to-image generation. *arXiv preprint arXiv:2403.04692*, 2024.
- Xiaoliang Dai, Ji Hou, Chih-Yao Ma, Sam Tsai, Jialiang Wang, Rui Wang, Peizhao Zhang, Simon Vandenhende, Xiaofang Wang, Abhimanyu Dubey, et al. Emu: Enhancing image generation models using photogenic needles in a haystack. *arXiv preprint arXiv:2309.15807*, 2023.
- Jiayu Ding, Shuming Ma, Li Dong, Xingxing Zhang, Shaohan Huang, Wenhui Wang, Nanning Zheng, and Furu Wei. Longnet: Scaling transformers to 1,000,000,000 tokens. *arXiv preprint arXiv:2307.02486*, 2023.
- Abhimanyu Dubey, Abhinav Jauhri, Abhinav Pandey, Abhishek Kadian, Ahmad Al-Dahle, Aiesha Letman, Akhil Mathur, Alan Schelten, Amy Yang, Angela Fan, et al. The llama 3 herd of models. *arXiv preprint arXiv:2407.21783*, 2024.
- Patrick Esser, Robin Rombach, and Bjorn Ommer. Taming transformers for high-resolution image synthesis. In *Proceedings of the IEEE/CVF conference on computer vision and pattern recognition*, pages 12873–12883, 2021.
- Patrick Esser, Sumith Kulal, Andreas Blattmann, Rahim Entezari, Jonas Müller, Harry Saini, Yam Levi, Dominik Lorenz, Axel Sauer, Frederic Boesel, et al. Scaling rectified flow transformers for high-resolution image synthesis. In *Forty-first International Conference on Machine Learning*, 2024.
- Lijie Fan, Tianhong Li, Siyang Qin, Yuanzhen Li, Chen Sun, Michael Rubinstein, Deqing Sun, Kaiming He, and Yonglong Tian. Fluid: Scaling autoregressive text-to-image generative models with continuous tokens, 2024. <https://arxiv.org/abs/2410.13863>.
- Yuying Ge, Sijie Zhao, Jingyu Zhu, Yixiao Ge, Kun Yi, Lin Song, Chen Li, Xiaohan Ding, and Ying Shan. Seed-x: Multimodal models with unified multi-granularity comprehension and generation. *arXiv preprint arXiv:2404.14396*, 2024.
- Dhruba Ghosh, Hannaneh Hajishirzi, and Ludwig Schmidt. Geneval: An object-focused framework for evaluating text-to-image alignment. *Advances in Neural Information Processing Systems*, 36, 2024.
- Rohit Girdhar, Mannat Singh, Andrew Brown, Quentin Duval, Samaneh Azadi, Sai Saketh Rambhatla, Akbar Shah, Xi Yin, Devi Parikh, and Ishan Misra. Emu video: Factorizing text-to-video generation by explicit image conditioning. *arXiv preprint arXiv:2311.10709*, 2023.
- Fabian Gloeckle, Badr Youbi Idrissi, Baptiste Rozière, David Lopez-Paz, and Gabriel Synnaeve. Better & faster large language models via multi-token prediction. *arXiv preprint arXiv:2404.19737*, 2024.
- Albert Gu and Tri Dao. Mamba: Linear-time sequence modeling with selective state spaces. *arXiv preprint arXiv:2312.00752*, 2023.
- Moayed Haji-Ali, Guha Balakrishnan, and Vicente Ordonez. Elasticdiffusion: Training-free arbitrary size image generation. *arXiv preprint arXiv:2311.18822*, 2023.
- Yingqing He, Shaoshu Yang, Haoxin Chen, Xiaodong Cun, Menghan Xia, Yong Zhang, Xintao Wang, Ran He, Qifeng Chen, and Ying Shan. Scalecrafter: Tuning-free higher-resolution visual generation with diffusion models. In *The Twelfth International Conference on Learning Representations*, 2023.
- Jack Hessel, Ari Holtzman, Maxwell Forbes, Ronan Le Bras, and Yejin Choi. Clipscore: A reference-free evaluation metric for image captioning. *arXiv preprint arXiv:2104.08718*, 2021.

- Martin Heusel, Hubert Ramsauer, Thomas Unterthiner, Bernhard Nessler, and Sepp Hochreiter. Gans trained by a two time-scale update rule converge to a local nash equilibrium. *Advances in neural information processing systems*, 30, 2017.
- Jonathan Ho and Tim Salimans. Classifier-free diffusion guidance. *arXiv preprint arXiv:2207.12598*, 2022.
- Jonathan Ho, Ajay Jain, and Pieter Abbeel. Denoising diffusion probabilistic models. *Advances in neural information processing systems*, 33:6840–6851, 2020a.
- Jonathan Ho, Ajay Jain, and Pieter Abbeel. Denoising diffusion probabilistic models. *Advances in neural information processing systems*, 33:6840–6851, 2020b.
- Angelos Katharopoulos, Apoorv Vyas, Nikolaos Pappas, and François Fleuret. Transformers are rnns: Fast autoregressive transformers with linear attention. In *International conference on machine learning*, pages 5156–5165. PMLR, 2020.
- Yuval Kirstain, Adam Polyak, Uriel Singer, Shahbuland Matiana, Joe Penna, and Omer Levy. Pick-a-pic: An open dataset of user preferences for text-to-image generation. *Advances in Neural Information Processing Systems*, 36: 36652–36663, 2023.
- Baiqi Li, Zhiqiu Lin, Deepak Pathak, Jiayao Li, Yixin Fei, Kewen Wu, Tiffany Ling, Xide Xia, Pengchuan Zhang, Graham Neubig, et al. Genai-bench: Evaluating and improving compositional text-to-visual generation. *arXiv preprint arXiv:2406.13743*, 2024a.
- Tianhong Li, Yonglong Tian, He Li, Mingyang Deng, and Kaiming He. Autoregressive image generation without vector quantization. *arXiv preprint arXiv:2406.11838*, 2024b.
- Tsung-Yi Lin, Michael Maire, Serge Belongie, James Hays, Pietro Perona, Deva Ramanan, Piotr Dollár, and C Lawrence Zitnick. Microsoft coco: Common objects in context. In *Computer Vision-ECCV 2014: 13th European Conference, Zurich, Switzerland, September 6-12, 2014, Proceedings, Part V 13*, pages 740–755. Springer, 2014.
- Zhiqiu Lin, Deepak Pathak, Baiqi Li, Jiayao Li, Xide Xia, Graham Neubig, Pengchuan Zhang, and Deva Ramanan. Evaluating text-to-visual generation with image-to-text generation. *arXiv preprint arXiv:2404.01291*, 2024.
- Yaron Lipman, Ricky TQ Chen, Heli Ben-Hamu, Maximilian Nickel, and Matt Le. Flow matching for generative modeling. *arXiv preprint arXiv:2210.02747*, 2022.
- Dongyang Liu, Shitian Zhao, Le Zhuo, Weifeng Lin, Yu Qiao, Hongsheng Li, and Peng Gao. Lumina-mgpt: Illuminate flexible photorealistic text-to-image generation with multimodal generative pretraining. *arXiv preprint arXiv:2408.02657*, 2024.
- Zhuoyan Luo, Fengyuan Shi, Yixiao Ge, Yujiu Yang, Limin Wang, and Ying Shan. Open-magvit2: An open-source project toward democratizing auto-regressive visual generation. *arXiv preprint arXiv:2409.04410*, 2024.
- Xiaoxiao Ma, Mohan Zhou, Tao Liang, Yalong Bai, Tiejun Zhao, Huaiyan Chen, and Yi Jin. Star: Scale-wise text-to-image generation via auto-regressive representations. *arXiv preprint arXiv:2406.10797*, 2024.
- Ben Mann, N Ryder, M Subbiah, J Kaplan, P Dhariwal, A Neelakantan, P Shyam, G Sastry, A Askell, S Agarwal, et al. Language models are few-shot learners. *arXiv preprint arXiv:2005.14165*, 1, 2020.
- Xichen Pan, Satya Narayan Shukla, Aashu Singh, Zhuokai Zhao, Shlok Kumar Mishra, Jialiang Wang, Zhiyang Xu, Juhai Chen, Kunpeng Li, Felix Juefei-Xu, et al. Transfer between modalities with metaqueries. *arXiv preprint arXiv:2504.06256*, 2025.
- William Peebles and Saining Xie. Scalable diffusion models with transformers. In *Proceedings of the IEEE/CVF International Conference on Computer Vision*, pages 4195–4205, 2023.
- Bo Peng, Eric Alcaide, Quentin Anthony, Alon Albalak, Samuel Arcadinho, Stella Biderman, Huanqi Cao, Xin Cheng, Michael Chung, Matteo Grella, et al. Rwkv: Reinventing rnns for the transformer era. *arXiv preprint arXiv:2305.13048*, 2023.
- Dustin Podell, Zion English, Kyle Lacey, Andreas Blattmann, Tim Dockhorn, Jonas Müller, Joe Penna, and Robin Rombach. Sdxl: Improving latent diffusion models for high-resolution image synthesis. *arXiv preprint arXiv:2307.01952*, 2023.
- Adam Polyak, Amit Zohar, Andrew Brown, Andros Tjandra, Animesh Sinha, Ann Lee, Apoorv Vyas, Bowen Shi, Chih-Yao Ma, Ching-Yao Chuang, et al. Movie gen: A cast of media foundation models. *arXiv preprint arXiv:2410.13720*, 2024.
- Alec Radford. Improving language understanding by generative pre-training. 2018.

- Alec Radford, Jong Wook Kim, Chris Hallacy, Aditya Ramesh, Gabriel Goh, Sandhini Agarwal, Girish Sastry, Amanda Askell, Pamela Mishkin, Jack Clark, et al. Learning transferable visual models from natural language supervision. In *International conference on machine learning*, pages 8748–8763. PMLR, 2021.
- Aditya Ramesh, Prafulla Dhariwal, Alex Nichol, Casey Chu, and Mark Chen. Hierarchical text-conditional image generation with clip latents. *arXiv preprint arXiv:2204.06125*, 1(2):3, 2022.
- Jingjing Ren, Wenbo Li, Haoyu Chen, Renjing Pei, Bin Shao, Yong Guo, Long Peng, Fenglong Song, and Lei Zhu. Ultrapixel: Advancing ultra-high-resolution image synthesis to new peaks. *arXiv preprint arXiv:2407.02158*, 2024.
- Robin Rombach, Andreas Blattmann, Dominik Lorenz, Patrick Esser, and Björn Ommer. High-resolution image synthesis with latent diffusion models. In *Proceedings of the IEEE/CVF conference on computer vision and pattern recognition*, pages 10684–10695, 2022.
- Chitwan Saharia, William Chan, Saurabh Saxena, Lala Li, Jay Whang, Emily L Denton, Kamyar Ghasemipour, Raphael Gontijo Lopes, Burcu Karagol Ayan, Tim Salimans, et al. Photorealistic text-to-image diffusion models with deep language understanding. *Advances in neural information processing systems*, 35:36479–36494, 2022.
- Tim Salimans and Jonathan Ho. Progressive distillation for fast sampling of diffusion models. *arXiv preprint arXiv:2202.00512*, 2022.
- Wenzhe Shi, Jose Caballero, Ferenc Huszár, Johannes Totz, Andrew P Aitken, Rob Bishop, Daniel Rueckert, and Zehan Wang. Real-time single image and video super-resolution using an efficient sub-pixel convolutional neural network. In *Proceedings of the IEEE conference on computer vision and pattern recognition*, pages 1874–1883, 2016.
- Jiaming Song, Chenlin Meng, and Stefano Ermon. Denoising diffusion implicit models. *arXiv preprint arXiv:2010.02502*, 2020a.
- Jiaming Song, Chenlin Meng, and Stefano Ermon. Denoising diffusion implicit models. *arXiv preprint arXiv:2010.02502*, 2020b.
- Peize Sun, Yi Jiang, Shoufa Chen, Shilong Zhang, Bingyue Peng, Ping Luo, and Zehuan Yuan. Autoregressive model beats diffusion: Llama for scalable image generation. *arXiv preprint arXiv:2406.06525*, 2024a.
- Quan Sun, Yufeng Cui, Xiaosong Zhang, Fan Zhang, Qiying Yu, Yueze Wang, Yongming Rao, Jingjing Liu, Tiejun Huang, and Xinlong Wang. Generative multimodal models are in-context learners. In *Proceedings of the IEEE/CVF Conference on Computer Vision and Pattern Recognition*, pages 14398–14409, 2024b.
- Quan Sun, Qiying Yu, Yufeng Cui, Fan Zhang, Xiaosong Zhang, Yueze Wang, Hongcheng Gao, Jingjing Liu, Tiejun Huang, and Xinlong Wang. Emu: Generative pretraining in multimodality. In *The Twelfth International Conference on Learning Representations*, 2024c. <https://openreview.net/forum?id=mL8Q9OamV>.
- Chameleon Team. Chameleon: Mixed-modal early-fusion foundation models. *arXiv preprint arXiv:2405.09818*, 2024.
- Keyu Tian, Yi Jiang, Zehuan Yuan, Bingyue Peng, and Liwei Wang. Visual autoregressive modeling: Scalable image generation via next-scale prediction. *arXiv preprint arXiv:2404.02905*, 2024.
- Hugo Touvron, Thibaut Lavril, Gautier Izacard, Xavier Martinet, Marie-Anne Lachaux, Timothée Lacroix, Baptiste Rozière, Naman Goyal, Eric Hambro, Faisal Azhar, et al. Llama: Open and efficient foundation language models. *arXiv preprint arXiv:2302.13971*, 2023a.
- Hugo Touvron, Louis Martin, Kevin Stone, Peter Albert, Amjad Almahairi, Yasmine Babaei, Nikolay Bashlykov, Soumya Batra, Prajjwal Bhargava, Shruti Bhosale, et al. Llama 2: Open foundation and fine-tuned chat models. *arXiv preprint arXiv:2307.09288*, 2023b.
- Aaron Van Den Oord, Oriol Vinyals, et al. Neural discrete representation learning. *Advances in neural information processing systems*, 30, 2017.
- Xi Wang, Nicolas Dufour, Nefeli Andreou, Marie-Paule Cani, Victoria Fernández Abrevaya, David Picard, and Vicky Kalogeiton. Analysis of classifier-free guidance weight schedulers. *arXiv preprint arXiv:2404.13040*, 2024a.
- Xinlong Wang, Xiaosong Zhang, Zhengxiong Luo, Quan Sun, Yufeng Cui, Jinsheng Wang, Fan Zhang, Yueze Wang, Zhen Li, Qiying Yu, et al. Emu3: Next-token prediction is all you need. *arXiv preprint arXiv:2409.18869*, 2024b.
- Chengyue Wu, Xiaokang Chen, Zhiyu Wu, Yiyang Ma, Xingchao Liu, Zizheng Pan, Wen Liu, Zhenda Xie, Xingkai Yu, Chong Ruan, et al. Janus: Decoupling visual encoding for unified multimodal understanding and generation. *arXiv preprint arXiv:2410.13848*, 2024.

Enze Xie, Junsong Chen, Junyu Chen, Han Cai, Haotian Tang, Yujun Lin, Zhekai Zhang, Muyang Li, Ligeng Zhu, Yao Lu, et al. Sana: Efficient high-resolution image synthesis with linear diffusion transformers. *arXiv preprint arXiv:2410.10629*, 2024a.

Jinheng Xie, Weijia Mao, Zechen Bai, David Junhao Zhang, Weihao Wang, Kevin Qinghong Lin, Yuchao Gu, Zhijie Chen, Zhenheng Yang, and Mike Zheng Shou. Show-o: One single transformer to unify multimodal understanding and generation. *arXiv preprint arXiv:2408.12528*, 2024b.

Jiahui Yu, Xin Li, Jing Yu Koh, Han Zhang, Ruoming Pang, James Qin, Alexander Ku, Yuanzhong Xu, Jason Baldridge, and Yonghui Wu. Vector-quantized image modeling with improved vqgan. *arXiv preprint arXiv:2110.04627*, 2021.

Lijun Yu, José Lezama, Nitesh B Gundavarapu, Luca Versari, Kihyuk Sohn, David Minnen, Yong Cheng, Vighnesh Birodkar, Agrim Gupta, Xiuye Gu, et al. Language model beats diffusion–tokenizer is key to visual generation. *arXiv preprint arXiv:2310.05737*, 2023a.

Lili Yu, Bowen Shi, Ramakanth Pasunuru, Benjamin Muller, Olga Golovneva, Tianlu Wang, Arun Babu, Binh Tang, Brian Karrer, Shelly Sheynin, et al. Scaling autoregressive multi-modal models: Pretraining and instruction tuning. *arXiv preprint arXiv:2309.02591*, 2(3), 2023b.

Qihang Yu, Ju He, Xueqing Deng, Xiaohui Shen, and Liang-Chieh Chen. Randomized autoregressive visual generation. *arXiv preprint arXiv:2411.00776*, 2024.

Chunting Zhou, Lili Yu, Arun Babu, Kushal Tirumala, Michihiro Yasunaga, Leonid Shamis, Jacob Kahn, Xuezhe Ma, Luke Zettlemoyer, and Omer Levy. Transfusion: Predict the next token and diffuse images with one multi-modal model. *arXiv preprint arXiv:2408.11039*, 2024.

# Appendix

This supplementary material provides more implementation details, ablation studies, visualization results, discussions and limitations. We provide detailed implementations in Sec. A to provide more insights. We also present more studies and visualization results in Sec. B. Finally, we discuss the limitations and further work of Token-Shuffle in Sec. C.

## A Implemental Details

*Instability in training 2048 resolution* Training at resolutions of  $512 \times 512$  or  $1024 \times 1024$  is notably stable, with the loss consistently decreasing throughout the process. However, *training at very high resolutions, such as  $2048 \times 2048$ , often becomes unstable*, as evidenced by a significant increase in training loss after several thousand iterations, as illustrated in Fig. 11.

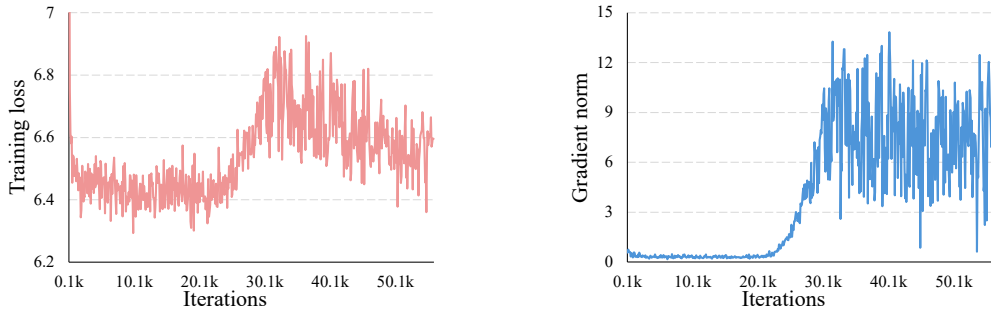


**Figure 11** We plot the *average loss* (left) and *gradient norm* (right) when training with a resolution of  $2048 \times 2048$ . Training shows instability after approximately 20K iterations.

To investigate the cause of unstable training, we analyze the training process in detail. Initially, we hypothesize that the instability arises from using a large learning rate, a common factor in such issues. To test this, we reduce the learning rate from  $1e^{-4}$  to  $5e^{-5}$  and  $1e^{-5}$ , decreasing it by factors of 2 and 10, respectively. However, the training instability persists, suggesting that the learning rate is not the root cause. Next, inspired by EMU3 Wang et al. (2024b), we consider that high-resolution images might cause visual tokens to dominate the training process. To address this, we apply a loss weight of 0.5 or 0.2 to the visual tokens. Unfortunately, this adjustment also fails to stabilize the training. We then investigate whether the logit shift issue, which has been observed to cause unstable training in larger models such as Chameleon Team (2024) and Lumina-mGPT Liu et al. (2024), could also occur in our 2.7B model. Notably, this phenomenon is typically associated with models containing 7B parameters or more. To tackle this, we consider two solutions: (1) incorporating QK-Norm into each attention layer, and (2) adding z-loss Team (2024) to the training objective. Empirically, we find that while QK-Norm partially alleviates the issue, the instability eventually recurs as training progresses. In contrast, z-loss effectively prevents instability throughout training. Thus, we combine both QK-Norm and z-loss to stabilize the training at  $2048 \times 2048$  resolution, and set the z-loss weight to  $1e^{-5}$ . Retrospectively, we emphasize that z-loss not only helps large models as indicated in Chameleon and Lumina-mGPT, but also helps very high-resolution image generation for discrete image generation pipeline.

*Inference Implementation* We consider both textual tokens and visual tokens for loss backpropagation, which has been empirically proven to be beneficial for text faithfulness. This approach trains both text and images, aligning with the philosophy of MLLMs, with the key difference being that we only use text-image paired datasets. However, during inference, the model (as with all autoregressive models) may (1) continue generating text instead of an image, or (2) produce mixed text-image tokens, resulting in incomplete images.

To address these issues, we first introduce a special token, `<|start_of_image|>`, appended to the end of prompt tokens. This ensures that the model always generates an image after the prompt. Without this token, the model may generate additional text as a supplement to simple prompts before concluding with an image, as shown in Fig. 12.

For mixed text-image tokens, we observe that during the early stages of training, the model is more prone to generating such outputs. However, as training progresses, the model consistently generates visual tokens up to the `<|end_of_image|>` token, resulting in complete images. In rare cases where this behavior does not occur, we enforce structural generation by restricting tokens following `<|start_of_image|>` to be sampled only from the visual vocabulary, ensuring the generation of complete images.



**Figure 12** Without explicitly appending `<|start_of_image|>` token, our model naturally generates text based on input and seamlessly transitions to an image, consistently and automatically concluding in line with training data format.

## B More Studies

### B.1 Choice of CFG scales

Conceptually, CFG enhances generation quality by balancing prompt fidelity with visual coherence. However, determining the optimal CFG scale is empirical and model-dependent [Girdhar et al. \(2023\)](#); [Sun et al. \(2024a\)](#); [Li et al. \(2024b\)](#); [Peebles and Xie \(2023\)](#); [Tian et al. \(2024\)](#). We systematically evaluate different CFG scales, ranging from 1.0 to 11.0, with VQAScore results presented in Fig.13 and illustrative examples shown in Fig.15. It is worth noting that no CFG schedulers were introduced in this study.

While a higher CFG scale generally leads to improved VQAScore, as demonstrated in Fig.13, we observe that

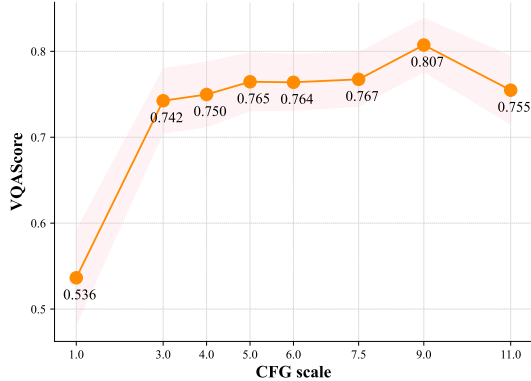


**Figure 13** CFG scale vs. VQAScore.

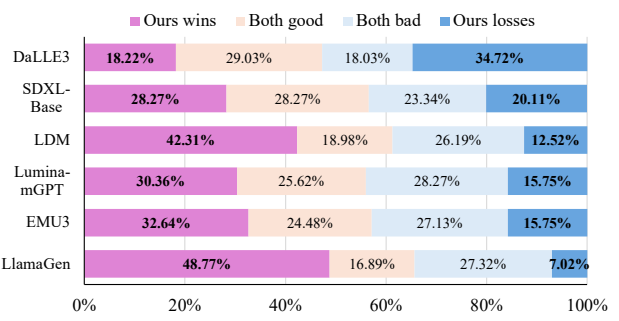


**Figure 14** Human evaluation of text alignment, comparing Token-Shuffle with various AR-based and diffusion-based models. Results may vary slightly from Fig. 6 due to the generated images are assessed by different vendors.

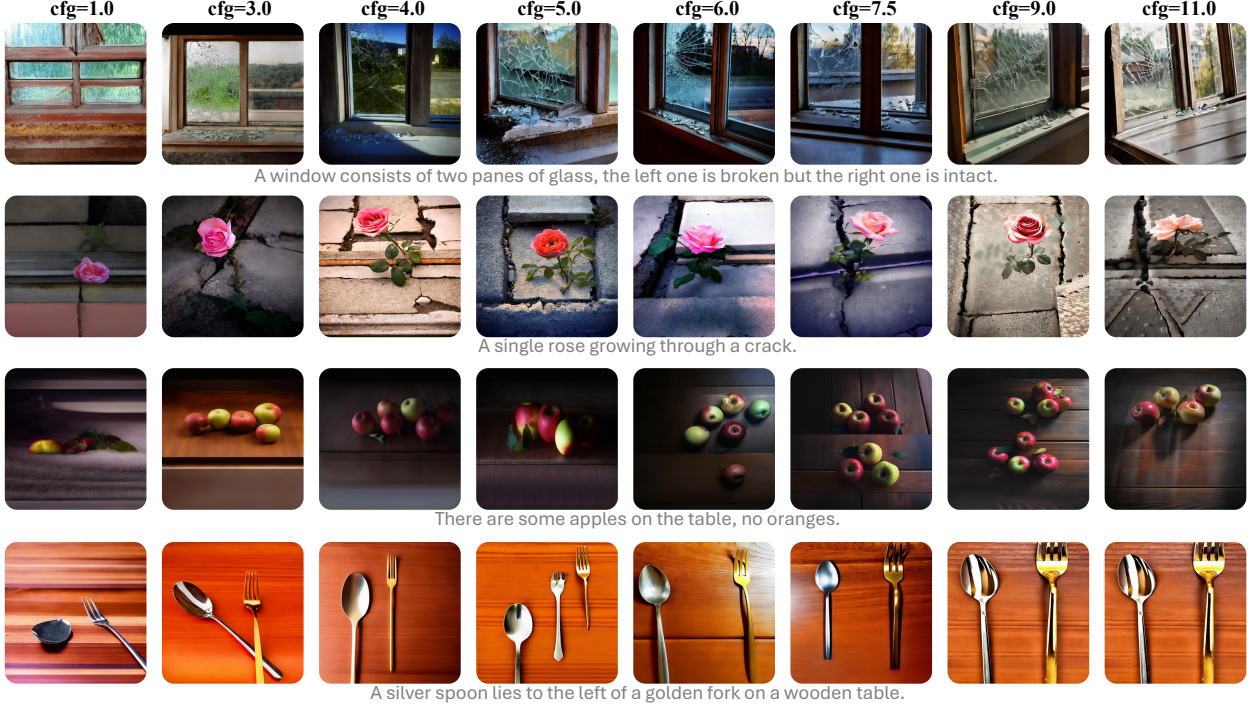


**Figure 15** Examples of generated images under different CFG scales.

it may also result in a slight deterioration of visual appearance, as illustrated in Fig.15. Taking into account both the qualitative and quantitative findings presented, we consider that a CFG value of 7.5 strikes the optimal balance between performance and visual quality.

## B.2 Text Alignment

We observe that our model delivers superior text-alignment performance, as demonstrated in the human evaluation results in Fig.6. To further substantiate this, we provide a detailed comparison, evaluating our method against additional models, with the corresponding human evaluation results presented in Fig.14. Our images are generated using a half-linear CFG scheduler with a scale of 7.5 and a fixed random seed.

Clearly, Token-Shuffle significantly outperforms all other methods by a considerable margin, except for DALL-E 3, which also trains and infers on long prompts. This experiment highlights the effectiveness of using long and detailed captions to improve text-to-image (T2I) text-faithfulness.

## B.3 Causal Attention Mask

*Token-Shuffle adheres to the standard next-token prediction mechanism without altering the original causal mask used in LLMs.* However, instead of predicting the next single token, it predicts a fused token, which is then disentangled into spatially local tokens. In this approach, the fused token retains the same causal mask as the LLM, but the disentangled tokens introduce a modified causal mask that allows mutual interactions within the spatial local window. Fig. 16 compares the attention maps of bi-directional, causal, and Token-Shuffle implementations.

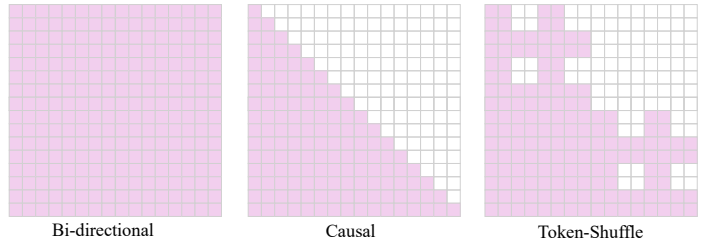


**Figure 16** Attention maps of three implementations: bi-directional, causal, and Token-Shuffle. Illustrated with a feature map size of  $4 \times 4$  (16 tokens) and a shuffle window size of 2 for Token-Shuffle.

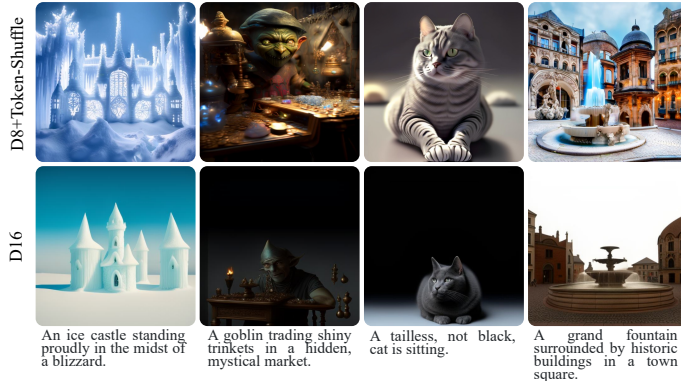


**Figure 17** Visual examples comparing Token-Shuffle (compress ratio 8 $\times$  with Token-Shuffle window size of 2) and high compress VQGAN (compress ratio 16 $\times$ ).

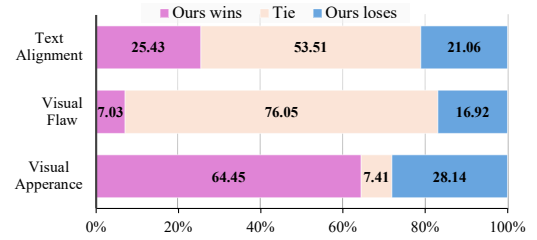


**Figure 18** Human evaluation of Token-Shuffle (compress ratio 8 $\times$  with Token-Shuffle window size of 2) and high compress VQGAN (compress ratio 16 $\times$ ).

While the bi-directional implementation facilitates global token interactions and the causal implementation enforces strict sequential constraints, Token-Shuffle strikes a balance by enabling local mutual interactions among tokens. This design is anticipated to improve visual generation quality, particularly in capturing finer local details, compared to the traditional causal design. Please note that this is achieved without altering the causal masking for both training and inference.

#### B.4 High-Compress VQGAN or Token-Shuffle

Token-Shuffle incorporates additional lightweight layers into Transformers to reduce the number of tokens, enabling efficient processing and high-resolution image generation. In contrast, some concurrent efforts in the diffusion model field, such as SANA Xie et al. (2024a), adopt a high-compression VAE image tokenizer strategy (*e.g.*, using a down-sampling ratio of 32 $\times$  rather than the more common 16 $\times$  or 8 $\times$ ). Here, we empirically explore and compare these two strategies (High-Compression Image Tokenizer *vs.* Token-Shuffle) and then discuss their potential limitations.

For the comparison, we utilize two VQGAN models with different compression ratios: 16 $\times$  and 8 $\times$ . The 16 $\times$  VQGAN model is taken from the previous LlamaGen T2I checkpoint, while the 8 $\times$  VQGAN is derived from our internal checkpoint. We first benchmark both models on the MSCOCO-val dataset Lin et al. (2014), which consists of 5K images. The images are resized and center-cropped to a resolution of 512  $\times$  512. The performance comparison of the VQGAN models is summarized in Tab. 3.

Clearly, a higher compression ratio significantly degrades reconstruction performance, which can negatively impact generation quality. Building on this observation, we investigate the generation quality of the two strategies using the aforementioned high- and low-compression VQGAN models. For this study, we generate 512  $\times$  512 resolution images, employing the 8 $\times$  compression ratio VQGAN with Token-Shuffle (shuffle window size of 2) to represent our Token-Shuffle strategy, and the 16 $\times$  compression ratio VQGAN to represent the high-compression image tokenizer approach. This setup ensures equivalent training and inference computational costs (excluding the negligible additional parameters and FLOPs introduced by Token-Shuffle). All images are generated using the same settings, including identical CFG values, temperature, CFG scheduler, *etc.* We evaluate and compare the two strategies on GenAI-Bench, reporting VQAScore and human evaluation results in Tab. 4 and Fig. 18, respectively.

Both auto-evaluation and human evaluation results unequivocally demonstrate that Token-Shuffle consistently outperforms its high-compression VQGAN counterpart. For illustration, we also provide visual examples

Ratio	Tokens	Codebook	PSNR	SSIM	CLIP
Low (8 $\times$ )	4096	8192	27.10	0.78	0.98
High (16 $\times$ )	1024	16384	22.89	0.64	0.96

**Table 3** Reconstruction results of VQGAN models with different compress ratios. The results are achieved on MSCOCO-val set with a resolution of 512.

Model	"Basic" prompts							"Hard" prompts						
	Attribute	Scene	Relation			Overall	Count	Differ	Compare	Logical		Overall		
			Spatial	Action	Part					Negate	Universal			
D16	0.80	0.82	0.79	0.79	0.86	0.80	0.72	0.71	0.73	0.65	0.75	0.71		
D8+TS	0.82	0.85	0.82	0.82	0.84	0.82	0.77	0.77	0.77	0.66	0.74	0.72		

**Table 4 VQAScore evaluation of image generation on GenAI-Bench.** "D16" indicates directly using a high-compress VQGAN with a down-sampling ratio of 16x. "D8+TS" indicates using a low-compress VQGAN with a down-sampling ratio of 8x and Token-Shuffle window size of 2.

in Fig. 17. However, we admit that this comparison is not entirely fair for the following reasons: (1) The image tokenizers were not trained under identical conditions, and it is challenging to obtain fairly trained VQGAN models with different down-sampling ratios. (2) During the course of our project, the dataset underwent slight and progressive changes—some images were added, while others were filtered out due to privacy concerns—affecting both pre-training and fine-tuning stages. Despite these factors, we believe they do not impact the validity of our conclusions.

In general, a higher-compression VQGAN offers the simplest implementation for supporting efficient and high-resolution image generation; however, it compromises generation performance, as shown in Tab.3, Tab.17, Fig.18, and examples in Fig.17. In contrast, Token-Shuffle, inspired by dimensional redundancy, introduces a pair of plug-and-play token operations that not only achieve superior generation performance and present better details but also provide dynamic settings for different shuffle window sizes, enabling adjustable compression results—a flexibility not available with high-compression VQGAN.

## B.5 More visual examples

We present additional visual examples in Fig.19 and Fig.20 to showcase the quality of  $1024 \times 1024$  generated images. Further examples of  $2048 \times 2048$  images are provided in Fig. 21. To our best knowledge, this is the first time AR-based models can generate such a high-resolution image efficiently and effectively. All images were generated with a shuffle window size of 2, half-linear CFG-scheduler with a scale of 7.5, as stated previously.

## C Discussions

### C.1 Visual Flaws of AR-based models

As discussed in Fluid Fan et al. (2024), AR-based models often produce images with visual flaws (see the human evaluation comparison with LDM in Fig.6 (c)). This issue stems not from the information loss in VQGAN but from the limited global interaction inherent to causal masking and the next-token prediction framework. Although Token-Shuffle introduces local mutual interactions, it still struggles with this fundamental limitation. Fig.5 shows examples of generated images with such visual flaws. Exploring approaches that maintain the next-token prediction framework while enabling global interactions remains an important direction for future research, with RAR Yu et al. (2024) offering a promising starting point.



**Table 5** Examples of generated images with visual flaws and structural errors, marked with red circle (zoom in to see details).

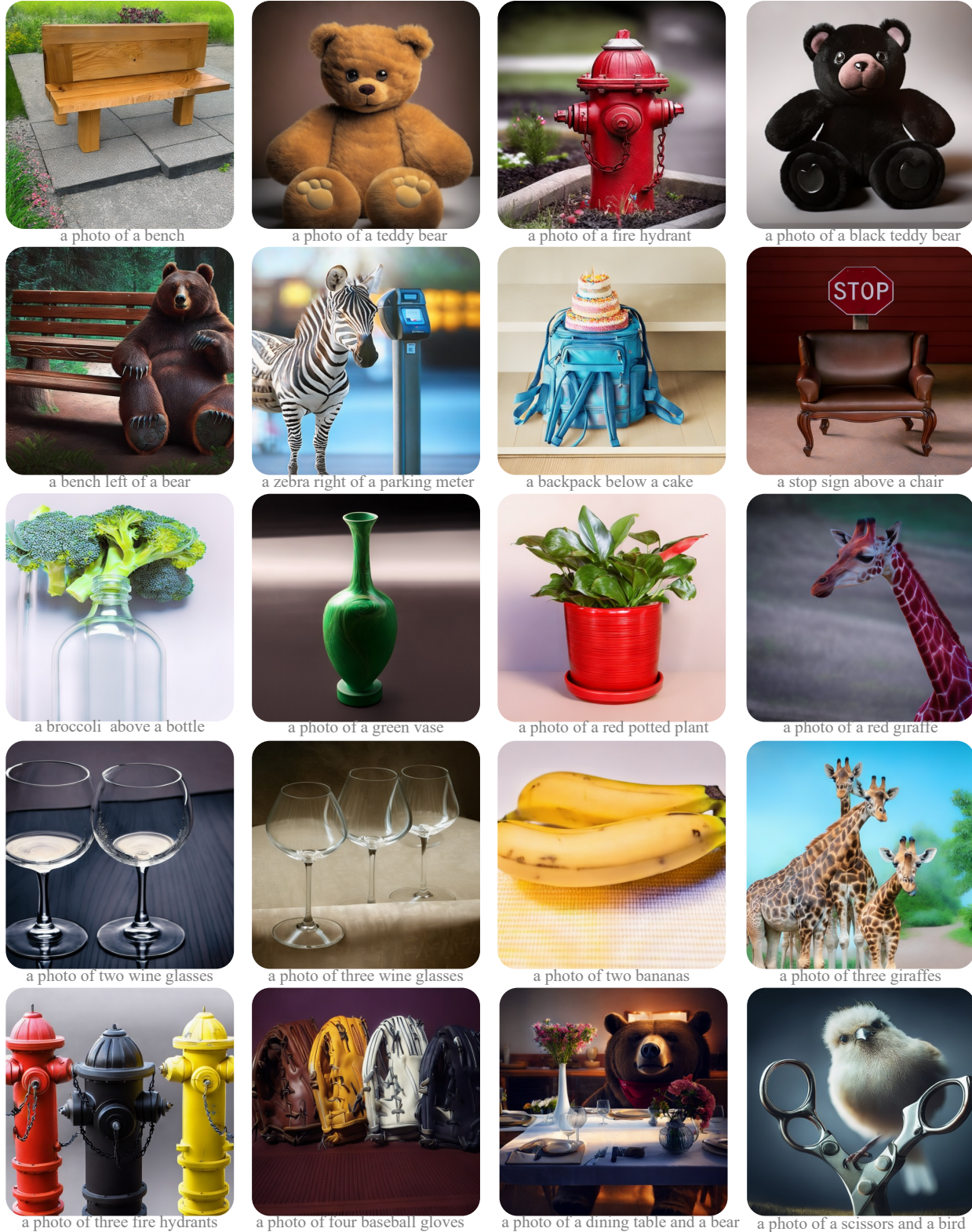


**Figure 19** 1024 × 1024 resolution images generated by Token-Shuffle with a shuffle window size of 2. We show generated images focusing on position, color, counting, and combination. The prompts are from GenEval Ghosh et al. (2024) prompts.

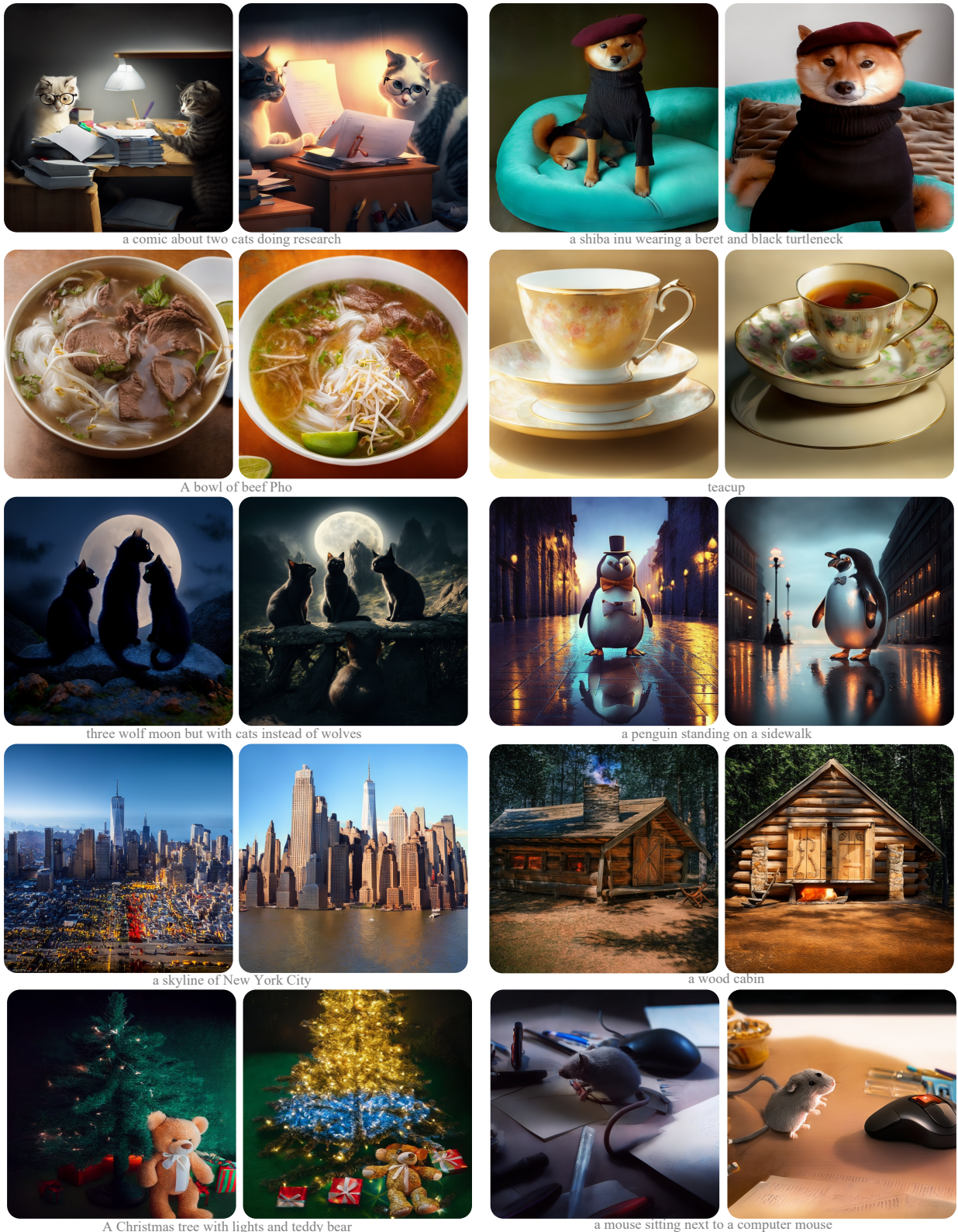


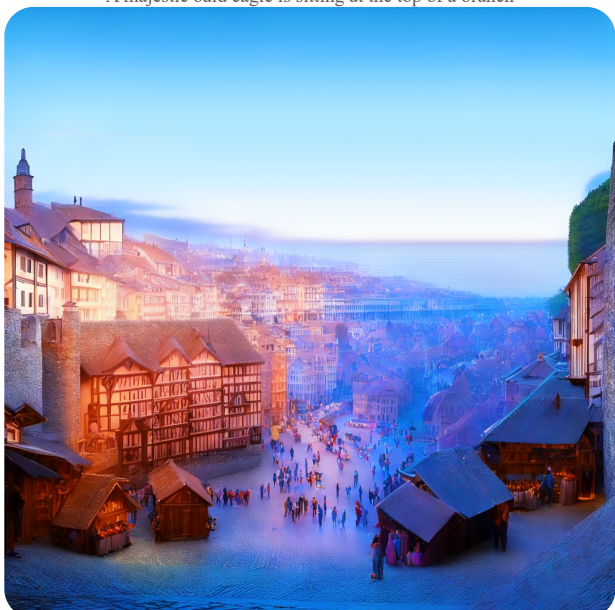
**Figure 20** 1024 × 1024 resolution images generated by Token-Shuffle with a shuffle window size of 2. We show two images of same prompt with different random seeds, focusing on complex scenarios or hard prompts. The prompts are from our internal evaluation prompts.



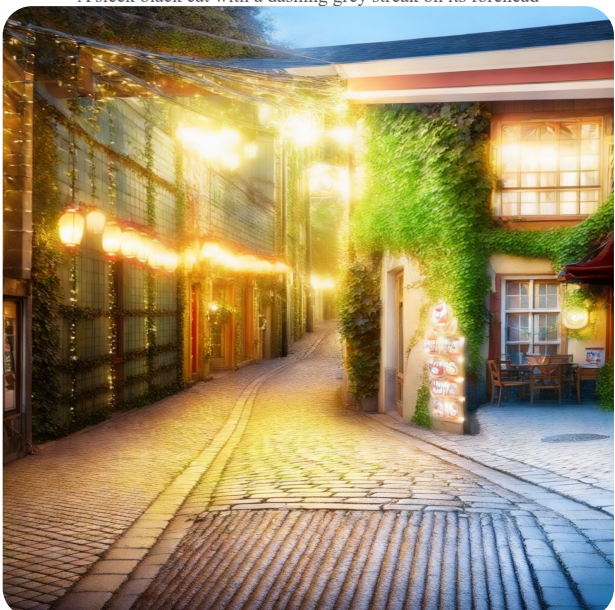
A majestic bald eagle is sitting at the top of a branch



A sleek black cat with a dashing grey streak on its forehead



A medieval town with market square



A narrow alleyway illuminated by strings of fairy lights, with their soft glow casting a warm ambience.

**Figure 21** 2048 × 2048 resolution images generated by Token-Shuffle with a shuffle window size of 2. Images are resized for visualization. Please zoom in to see the details in top row and the overall soft holistic beauty in bottom row.

## C.2 Limitations

We introduce Token-Shuffle, targeting efficient high-resolution image generation with AR models with high quality. However, there are still interesting directions worth exploring. Firstly, we would like to see the scaling ability of Token-Shuffle in large LLMs, *i.e.*, 7B and 30B models. We demonstrate that our 2.7B model is able to provide promising performance, outperforming 7B Lumina-mGPT, and can generate higher resolution. We expect better results when increasing the model size. Another interesting direction is to support flexible resolutions, aspect ratios like EMU3 [Wang et al. \(2024b\)](#).